energies

MDPI

Article

Experimental Determination of the Influence of Shape on the Heat Transfer Process in a Crushed Granite Storage Bed

Magdalena Nemś

Department of Thermodynamics and Renewable Energy Sources, Faculty of Mechanical and Power Engineering, Wroclaw University of Science and Technology, Wybrzeże Wyspiańskiego 27, 50-370 Wroclaw, Poland; magdalena.nems@pwr.edu.pl

Received: 8 November 2020; Accepted: 18 December 2020; Published: 20 December 2020

Abstract: The article presents the problem of modelling the charging of a constant-phase bed storage in the first hours of the process. The places of errors in the heat transfer calculations for the packed beds were indicated. Granite in the shape of spheres and crushed rocks, with a characteristic dimension of 50 mm, was used for the experimental tests. The material was subjected to tomographic examination and then used as a storage material. The charging process was carried out for three flow rates: 0.006, 0.008 and 0.010 m^3/s. After three hours of testing, the temperature of the outlet air for the granite sphere as the storage material was the same as for the granite crushed rock. However, the biggest differences occurred after 1 h of charging. They were equal to: 40.4% for the flow rate of 0.006 m^3/s, 22.0% for the flow rate of 0.008 m^3/s, and 18.5% for the flow rate of 0.010 m^3/s. The differences were greater than the uncertainty of the measurements. As a result, different temperatures of the storage material were obtained. After three hours, they were equal to: 25.2%, 12.3% and 8.6% for the lowest, medium, and highest airflow, respectively. The conducted heat transfer analysis and the relationship $Nu = f(Re)$ was determined. The influence of the calculated and actual surface of the crushed rock on the heat exchange process was explained. For all the tested air flow rates through the bed, higher thermal parameters were obtained for the crushed rock than for the sphere. The maximum differences in the Nu number were: 222.6%, 151.4% and 161.3% for the flow of 0.006, 0.008 and 0.010 m^3/s, respectively. This means that the description of the heat exchange process in the piled beds would require a parameter that takes into account the geometry of the storage material.

Keywords: heat storage; sensible heat; heat transfer; rock bed storage; rock shape

1. Introduction

Rock beds are a good and cheap alternative to complex and expensive heat storages, especially for those that cooperate with solar collectors [1]. Their advantages, apart from their price, also include the ability to work in a wide range of temperatures. The use of heat storages filled with rocks has been the subject of many research works conducted from the middle of the last century [2], which is confirmed by the number of papers from that period that are still quoted in current literature reviews [3]. Due to the wide use of renewable energy, and the seeking of savings through the recovery of waste heat, the amount of research and installations using rocks as a heat bed storage is still growing [4]. The research results show that constant-phase bed storages achieve similar efficiencies to phase-change bed storages, however, they are characterized by a lower investment cost [5]. They are used in solar power plants [6], in buildings for room heating or for the drying of premises [7], as a part of solar dryers [8], in greenhouses to ensure the right temperature for plants [9], as waste heat storages, or in cooperation with the Organic Rankine Cycle [10]. In such installations, air dominates as the working

medium [11], and other working factors, such as e.g., synthetic heat transfer fluid that is based on eutectic mixtures, are less frequently analysed [12]. The latest research [13] also highlighted an issue concerning the intensification of the heat transfer with the use of spherical material that has pores of a different diameter and depth on its surface.

The intensity of the charging process of heat storage plays an important role, especially during its cooperation with a heat source that is available for a short time. This is the case when e.g., a solar installation is operating after the summer season, or in a geographic location with moderate sunshine, such as Central Europe, which is characterized by a temperate climate and a high variability of weather conditions.

Previous experimental studies, which concerned a granite bed storage and which were carried out by the author of this paper, showed a different nature of the storage process in relation to the shape of the tested material [14]. Different characteristics of the working medium's outlet temperature from the heat storage were obtained for the same testing conditions. For the crushed granite filling, the air outlet temperature was lower than the temperature of the granite in the form of spheres and cubes. In addition, the discharge temperature curve was of a different nature, which was especially visible in the first two hours of the bed storage's charging process. Such a situation occurred despite the fact that the tested elements had the same equivalent diameter [15]. Due to these discrepancies, the author of the paper decided to continue research on crushed granite as a filling material. The quoted studies show a high intensification of the heat storage process in the bed storage filled with crushed stone. The differences related to the shape of the filling material are difficult to theoretically describe. This is due to the fact that in order to create mathematical models for the process of heat storage in a rock storage bed, it is necessary to use the characteristic dimension. In the case of packed storage beds, this dimension is the equivalent diameter of the material, which regardless of its shape, is treated as a sphere. Literature provides formulas for the Nusselt number to determine the heat transfer coefficients to the material, which are developed e.g., by Ranz and Marchall [16], Kacnelson and Timofiejewa [17], or Ketterning [18]. In these formulas, in the case of spheres, their diameter is taken as the characteristic dimension. However, for other geometries it is an equivalent diameter calculated from the volume of the sphere. Such simplifications were also adopted in more recent studies. R. Singh et al. in [19] used the equivalent diameter in the case of calculating a bed storage filled with large elements such as cubes and cuboids. H. Singh et al. also used the equivalent diameter to investigate a sphere and 4 different cuboids [20]. K.G. Allen et al. in [21] used the equivalent particle diameter for the analysis of crushed rock. When analyzing pressure drops for various other filling materials, regardless of their shape, the authors determined the equivalent diameter with regards to particle volume and surface area [22]. Similarly, N.G. Barton in [23] used the spherical diameter of individual rock particles. Jean-Francois P. Pitot de la Beaujardiere et al. in [24] used the mean equivalent particle diameter for a rock bed thermal energy storage system in CSP plants.

It is also worth noting that most of the studies concerning rock bed storages that are available in literature assume a long charging time, which even exceeds several hours [25] and can take up to one year [26]. This is due to the fact that these solutions are mainly dedicated to solar power plants [27], which are built in places with a high availability of solar radiation, and which operate continuously during the day. Among the experimental tests on a laboratory scale, the following charging times can be found:

- 6 h of charging [28]—test stand with rocks. Swedish diabase and magnetite were tested as the filling material, and the working medium was air.
- 8 h of charging [29]—laboratory test stand for testing the operation of the bed storage with parameters as in the case of concentrated solar power plants when combined with the Brayton cycle. The working medium was air.
- 8 h of charging [30]—the potential of quartzite and flint rocks as filler materials was investigated experimentally.

Analyses concerning long charging times also dominate in theoretical research:

- 6 h [23]—charging of a rock bed. The research covered issues related to air distribution during charging and discharging.
- 8 h [31]—charging of a bed storage intended for a solar thermal power plant. The working medium was air.
- 8 h [32]—charging the bed storage of a solar thermal power plant. The authors conducted thermodynamic modelling and performed exergy analysis. They used air.

The latest research [33] also shows a several-hour charging process in which crushed rock was used. A mathematical model for the bed storage was made and compared with the results of the experiment. The largest discrepancies were obtained in the first 3 h of charging. After this time, the outlet temperature values for the experiment and the model began to coincide.

It is difficult to find studies in literature in which short charging times are shown. Such studies are described in [34]. Measurements for the charging time of 170 min were used to create a one-dimensional numerical model, which enables the temperature of the storage material to be determined.

In studies in which the bed storage's charging process is long, it is difficult to observe the course of the characteristics for the first hours of charging, as well as to analyze the cooperation of the bed storage with a heat source that is available for a short time. In the mathematical description of the process of heat exchange between the working medium flowing through the bed storage and the storage material, there are significant simplifications. The sphere has the smallest surface area of all solids. However, in heat transfer calculations, it is assumed that the surface of e.g., crushed rock, is like a sphere. Such an assumption means, in model calculations, that the storage material in the form of spheres and crushed stone will equally absorb heat from the working medium. The author noted, in the studies described in [15], that there are significant differences in the charging of a bed storage filled with spheres and those filled with crushed rock. The obtained differences in the 1st and the 2nd law efficiency show that the geometry of the rock has an impact on the heat transfer process. According to the author, the assumption that the heat transfer process for crushed rock can be described by equations for spheres is incorrect. This is especially visible in the case of short charging times.

The author of the paper wants to show that there are significant differences in the first hours of charging a bed storage filled with a material of a different shape, despite the same characteristic dimension. As shown in the analysis of literature, research concerning the short charging time of a bed storage is the subject of a few studies, and therefore the process of heat transfer by the storage material is insufficiently described. Moreover, the author wants to show the influence of the actual surface area of the material on the Nusselt number, which describes the process of heat penetration into the storage material.

2. Materials and Methods

In order to determine the influence of the shape of crushed rock on the heat transfer process, it was necessary to prepare the material for research. The criterion equations for the determination of the Nusselt number Nu assume that the material placed in the bed storage is treated as spheres. Therefore, spheres were used as the model geometry in the research, and they were then compared to crushed rock. The material was mechanically processed and then placed inside the bed storage. Measurements were made during the charging of the heat storage, and the compared test results of the obtained criterion numbers for spheres and crushed rock provided information concerning the influence of shape on the heat exchange process. The analyses included the case in which the Nusselt number determined for the crushed rock takes into account its real surface area, as well as when this area is calculated as the area for a sphere.

2.1. Preparation of the Material for Research

In order to prepare the material for testing, its properties were determined. Granite from an excavation in Strzegom (Poland) was used. It specific heat is 780 J/(kg·K), and density 2659 kg/m^3. This rock was machined in order to obtain the shape of smooth spheres with a diameter of 50 mm. In this way, n = 230 pieces were obtained, with a mass m_{mat} = 174 g each. The same number of crushed rock pieces of the same weight was then selected. They were cleaned and sent for tomographic examination (Figure 1) in order to precisely determine their surfaces. These tests were performed by an external company using the X-ray Computed Tomography method and a tomograph: Nikon XT H 225, lamp: Rotating Target 225 kV, detector: Varex 4343.

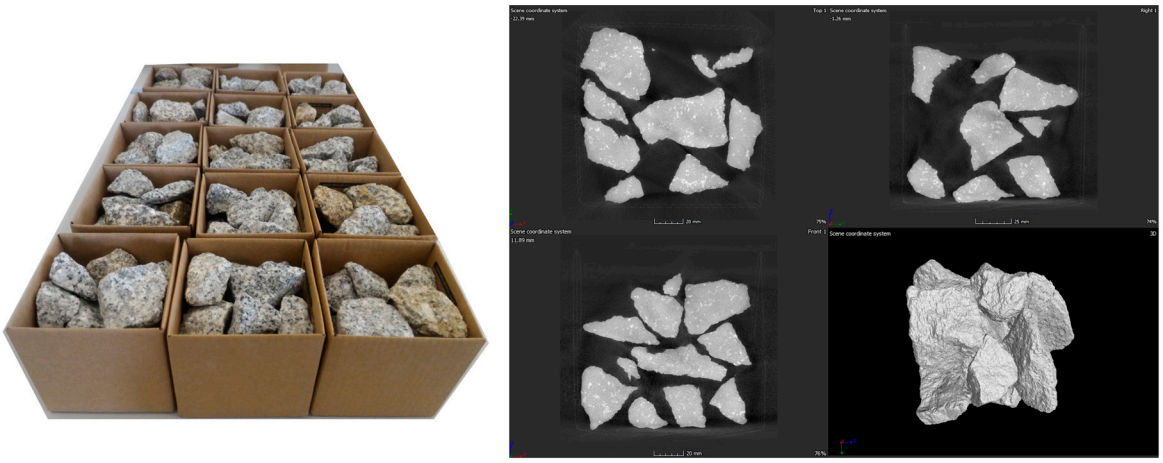

Figure 1. Material prepared for tomographic examination and exemplary scans of the granite crushed rock.

The material used for the tests had different levels of roughness. For the spheres it was from 3.94 to 23.57 µm, and for the crushed rock it was from 79.22 to 276.61 µm (see Figure 2). The tests were performed using the KEYENCE VHX Microscope.

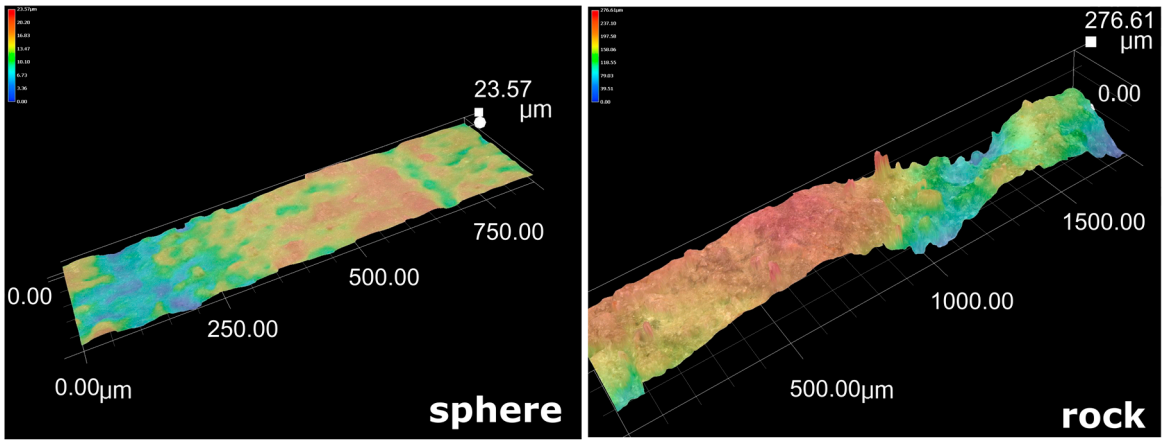

Figure 2. Roughness of the granite sphere and crushed rock.

Knowing the mass m_{mat} of the material, and its density ρ_{mat}, the volume V_{mat} can be determined using formula (1).

$$V_{mat} = \frac{m_{mat}}{\rho_{mat}} \quad (1)$$

The diameter of the material D_{mat} is determined from the volume (2). For the sphere, this is its actual diameter. However, for the crushed rock it is called the equivalent diameter.

$$D_{mat} = \sqrt[3]{\frac{6 \cdot V_{mat}}{\pi}} \tag{2}$$

By knowing the diameter of a single filling material D_{mat}, its surface area S_{sphere} can be calculated from the formula for the surface area of a sphere (3).

$$S_{sphere} = 4 \cdot \pi \left(\frac{D_{mat}}{2} \right)^2 \tag{3}$$

The results of calculations and tomographic tests are presented in Table 1. For elements in the form of crushed rock, two values of its surface are given. The first theoretical one, calculated from formula (3), assumes its sphericity. The second is the real surface obtained from the tomographic examinations. The difference between the theoretical area (calculated as for a sphere) and the actual value of the crushed rock is equal to 28.6%.

Table 1. Summary of characteristic data of the filling material.

Shape of Material	Equivalent Diameter	Surface Area
sphere	0.05 m	0.00785 m^2
crushed rock (treated as a sphere)	0.05 m	0.00785 m^2
crushed rock	0.05 m	0.010983 m^2

2.2. Test Stand and Experimental Research

The test stand shown in Figure 3 was used for the experimental research. The working medium was forced by the air fan to the flow meter, and then to the bed storage. Before entering the bed storage, the air was heated with an electric heater to a set temperature according to the test plan. The air flow rate and the temperature of the medium were regulated with the use of autotransformers connected with a fan and an electric heater, respectively. The inlet and outlet air temperature, and also the ambient temperature were measured with Pt100 thermocouples. A KD7 recorder with a one-minute step was used for data recording. This causes the uncertainty of the time measurement to be very small, because it results only from the accuracy of the KD7 recorder timer. Moreover, the pressure difference at the inlet and outlet of the bed storage was also recorded.

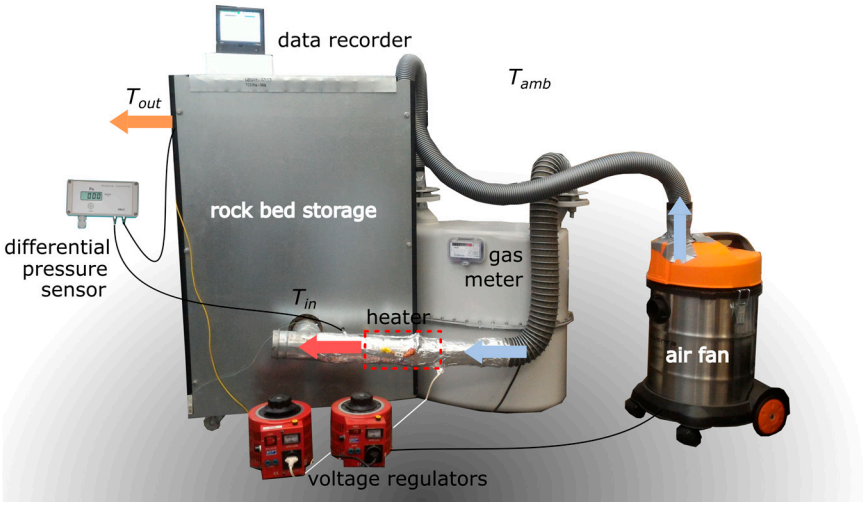

Figure 3. Experimental stand for the investigation of the heat storage process.

The crushed rock shaped and sphere shaped storage material was laid loosely inside the bed storage, as shown in Figure 4. Due to the same weight of the filling, which is equal to 40.02 kg, the same fill factor of 65.2% was obtained.

Figure 4. Crushed rock and spheres arranged inside the bed storage.

The dimensions of the bed storage, the used insulation and the data concerning the filling are summarized in Table 2. During the tests, the air directed to the bed storage was heated to the temperature $T_{air\_in} = 110°C$ by a heater in order to simulate the operation of a heat source, which may be an air solar collector. The tests were performed for three measurement series for each geometry, with the air flow rate through the heat storage being regulated. The setting values for the successive series of measurements are presented in Table 2.

Table 2. Parameters of the test stand and the filling material.

Rock bed	Internal height	0.5 m
	Internal thickness	0.3 m
	Internal length	0.3 m
Storage material	Equivalent sphere diameter	0.50 m
	Number of elements	230
	Mass	40.02 kg
Air	Inlet temperature	110 °C
	Volumetric flow rate 1	0.0060 m^3/s
	Volumetric flow rate 2	0.0080 m^3/s
	Volumetric flow rate 3	0.0100 m^3/s
Insulation	Top insulation thickness	0.20 m
	Bottom insulation thickness	0.15 m
	Side insulation thickness	0.15 m
	Thermal conductivity	0.039 W/(m·K)

The volumetric airflow rate was determined with an accuracy of ±0.0007 m^3/s. The initial temperature of the storage material depended on the ambient temperature. Table 3 shows the temperature in the laboratory, which was assumed as the granite's temperature at the beginning of the charging process.

Table 3. The ambient temperature in the laboratory.

Volumetric Flow Rate, m^3/s	Shape of Material	Initial Temperature, °C
0.006	granite sphere	19.1
	crushed granite	19.0
0.008	granite sphere	21.6
	crushed granite	20.8
0.010	granite sphere	19.0
	crushed granite	19.2

The air flow rate that is suitable for the cooperation with solar air collectors, in which the developed surfaces were used, was selected [35,36]. This enables a high efficiency of solar systems to be obtained when energy expenditure for the pumping of the medium is low.

2.3. Determination of the Characteristic Numbers

Experimental tests of the heat storage charging process were performed for two different types of filling and three air flow rates. According to the adopted convention when conducting such measurements, which was presented in all the experiments described in the literature review, one measurement series was performed for each of the settings. The charging time was set to 3 h. This is the time in which the outlet air temperature T_{air_out} changes dynamically. It is also the time of charging the bed storage during its cooperation with a heat source that is available for a short time, which has not been described well enough in literature. Figure 5 shows the change in the outlet air temperature over time for the spheres and crushed rock granite. The accuracy of the temperature measurement resulted from the accuracy of the used thermocouples and was equal to ±1.5 °C.

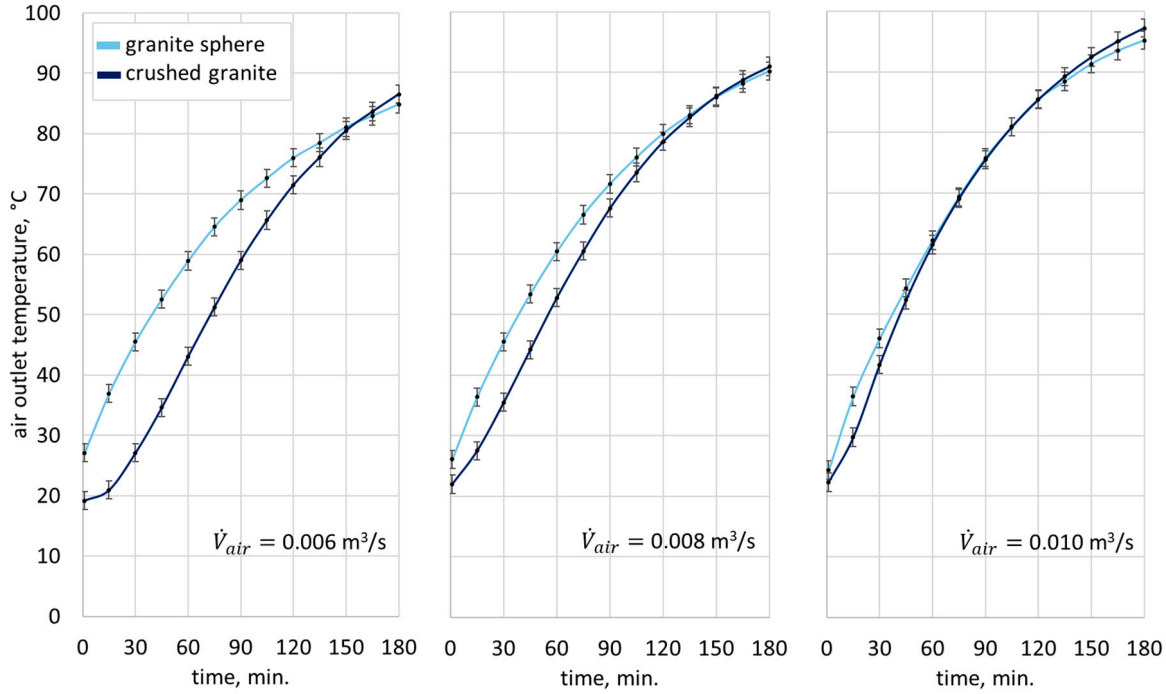

Figure 5. The temperature of the outlet air during the charging process of the bed storage for different air flow rate values.

Figure 5 shows the differences in the values of outlet air temperature for the spheres and crushed rock. This means that the heat exchange process between air and granite is of a different nature, during the first three hours of charging. The greatest differences in the outlet temperature for the sphere and crushed rock are equal to 18.4 °C for the smallest flow, 10.0 °C for the medium flow, and 6.8 °C for the highest flow. Due to the accuracy of the temperature readings, which is equal to ±1.5 °C for each of the measurements, the maximum error for the given differences is 3 °C. This means that the obtained discrepancies are not the result of inaccurate temperature measurements. Therefore, it is important to determine the heat transfer rate between the air flowing through the bed storage and the granite. The heat transfer coefficient needs to then be determined. In order to describe the process in detail, the heat transfer process should be characterized as a function of the flow rate. For this purpose, it is useful to calculate the characteristic numbers for the flow of fluid and the heat transfer.

The Reynolds number for the airflow through the storage material is determined from general Equation (4).

$$Re = \frac{D \cdot w_{air}}{\nu_{air}} \tag{4}$$

The velocity of the airflow w_{air} inside the bed storage through which the air flows is calculated from the volumetric flow rate $\dot{V}_{air}$ and the actual bed's cross-section A_{real} (5).

$$w_{air} = \frac{\dot{V}_{air}}{A_{real}} \tag{5}$$

The actual cross-sectional area of the bed storage through which the air flows takes into account the area occupied by the storage material, and therefore formula (6) takes the following form.

$$A_{real} = \frac{V_{real}}{b} \tag{6}$$

Parameter b is the internal height of the bed storage, which according to Table 2 takes the value of 0.5 m. The real volume inside the bed V_{real} determines the free space through which the air flows, and according to (7) it is the difference between the total volume of the bed storage V_{bed} and the volume occupied by the storage material V_{accu}.

$$V_{real} = V_{bed} - V_{accu} \tag{7}$$

Therefore, the final actual volume inside the bed V_{real} can be written as (8)

$$V_{real} = a^2 \times b - n \times V_{mat} \tag{8}$$

where parameter a is the internal width of the bed storage (see Table 2). The kinematic viscosity ν_{air} for air is determined for the average air temperature inside the bed storage T_{avg}, and is described by Equation (9) [37].

$$\nu_{air} = 8.461 \times 10^{-11} \times {T_{avg}}^2 + 9.348 \times 10^{-8} \times T_{avg} + 1.323 \times 10^{-5} \tag{9}$$

The Nusselt number Nu describing the process of heat transfer into the storage material can be represented by Equation (10) [38].

$$Nu = \frac{h_{mat} \times D_{mat}}{\lambda_{air}} \tag{10}$$

The thermal conductivity λ_{air} was determined for the average air temperature inside the bed storage T_{avg} according to (11) [37].

$$\lambda_{air} = -5.630 \times 10^{-8} \times {T_{avg}}^2 + 7.519 \times 10^{-5} \times T_{avg} + 2.420 \times 10^{-2} \tag{11}$$

Parameter h_{mat} is the heat transfer coefficient from the air flowing through the bed storage to the storage material. It is determined from the amount of heat transferred from the air flowing to the granite according to (12).

$$h_{mat} = \frac{\dot{Q}_{accu}}{n \times S_{sphere} \times \left(T_{avg} - T_{mat}\right)} \tag{12}$$

The temperature of material T_{mat} is a parameter obtained using the heat balance of the bed storage, which can be written as (13).

$$\dot{Q}_{accu} = \dot{Q}_{in} - \dot{Q}_{loss} \tag{13}$$

In the case of the heat supplied to the bed storage, the heat transfer rate $\dot{Q}_{in}$ is determined from (14) [39].

$$\dot{Q}_{in} = \dot{V}_{air} \times \rho_{air} \times c_{p\_air} \times (T_{air\_in} - T_{air\_out}) \quad (14)$$

In Equation (14), the specific heat at a constant pressure c_{p_air} is calculated for the average air temperature inside the bed storage T_{avg} using Equation (15) [37].

$$c_{p\_air} = 2.526 \times 10^{-10} \times {T_{avg}}^5 - 1.459 \times 10^{-7} \times {T_{avg}}^4 + 2.783 \times 10^{-5} \times {T_{avg}}^3 - 1.317 \times 10^{-3} \times {T_{avg}}^2 + 1.901 \times 10^{-2} \times T_{avg} + 1.005 \times 10^3 \quad (15)$$

The rate of heat losses from the surface of the bed storage to the environment $\dot{Q}_{loss}$ were determined as the sum of heat transfer rates passing through each surface of the bed storage. Figure 6 shows all the parameters that were used to calculate these heat losses. The computational algorithm numerically solved a total of 26 equations. It was described in detail by the author in [15].

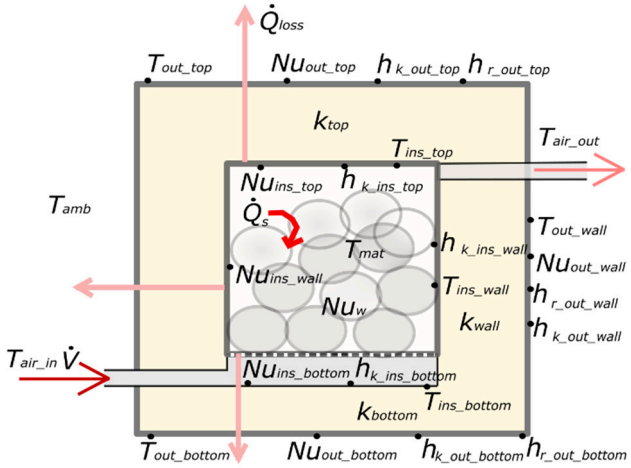

Figure 6. Diagram of the heat bed storage, with the thermal and material parameters marked.

The calculation algorithm presented in this chapter enabled the following parameters to be determined: flow parameters, such as: air velocity in the bed storage w_{air}, and the Reynold number Re, as well as thermal parameters, such as: the heat transfer rate between the flowing air and the storage material $\dot{Q}_{accu}$, the heat transfer coefficient into the material h_{mat}, and the Nusselt number Nu.

3. Results

During the conducted tests, the drop in pressure inside the storage bed was measured. The pressure losses for the spheres and crushed rock were the same in the case of a constant flow rate. They were equal to 2.9 Pa for the flow of 0.006 m^3/s, 5.0 Pa for the flow of 0.008 m^3/s. and 7.2 Pa for the flow of 0.010 m^3/s. The accuracy of the measurement, related to the accuracy of the device, was equal to ±0.5 Pa. Due to the obtained low values of pressure drops when compared to the amount of accumulated heat, they were not analysed further in the study.

The heat exchange between the air flowing through the bed storage and the storage material affects the amount of heat transfer rate. As a result, the temperature of the granite increases. Figure 7 shows the heat transfer rate and the average temperature of the material filling the bed storage, which was calculated from the heat balance.

The changes in the heat transfer rates visible in Figure 7 show the dynamics of the process during 3 h of charging the bed storage. The greatest differences in the heat transfer rates for the sphere and the crushed rock are for the smallest flow rate. This results in a different temperature of granite. These differences are the greatest in the first hour of charging and they decrease during the measurements.

The values of the temperature of the storage material after three hours of charging are summarized in Table 4.

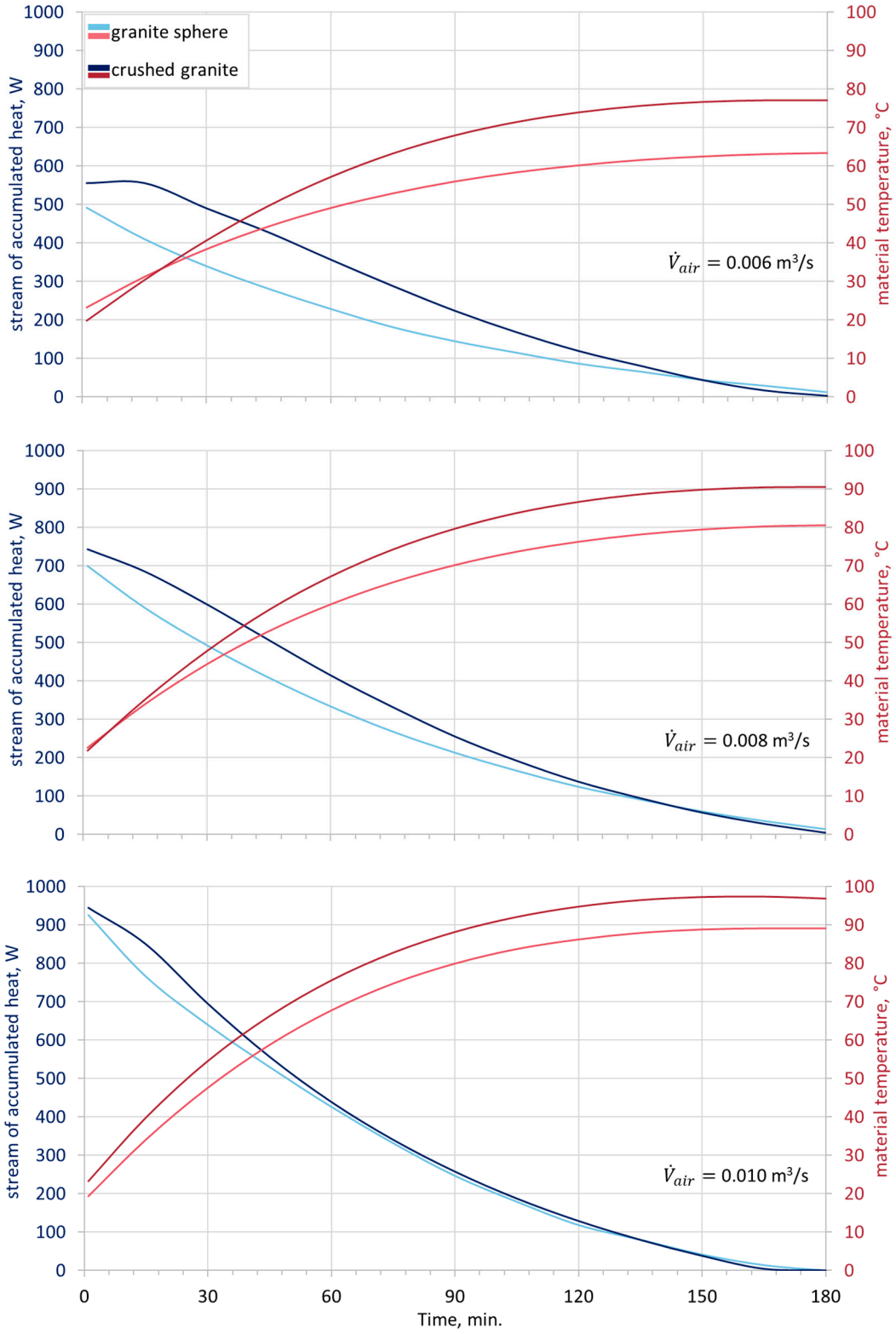

Figure 7. The heat transfer rate and the temperature of granite over time.

Table 4. The temperature of the storage material after three hours of charging.

Volumetric Flow Rate, m^3/s	Shape	Final Temperature, °C
0.006	granite sphere	63.4
	crushed granite	79.4
0.008	granite sphere	80.6
	crushed granite	90.5
0.010	granite sphere	89.2
	crushed granite	96.9

It is worth noting that with an increase in the airflow rate, these differences are decreasing. However, for the highest flow rate, the heat transfer rates are also the highest. Therefore, in order to better assess the intensity of heat transfer, it is worth analysing the characteristic numbers that describe the heat transfer process.

The efficiency of the heat accumulation process is influenced by the heat loss from the surface of the bed storage and the heat taken up by the storage material. The first of these heats can be significantly reduced. One of the basic criteria for improving efficiency is the economic aspect, which results from the increase of the amount of insulation material. The second heat is related to the process parameters, such as: flow rate or temperature difference, as well as to the material parameters, such as: the diameter of a single storage material or its surface. In order to analyse the heat transfer process, it is worth paying attention to the Nusselt number, which is considered as the characteristic number that is appropriate for the characterization of the heat being transferred to the storage material. This number takes into account the above parameters and allows the heat transfer process for different process conditions to be compared.

The performed measurements allowed the *Nu* number for the charging process of the bed storage filled with spheres and crushed rock to be determined. In order to specify the *Nu* number for the crushed rock, the surface area calculated from the equivalent diameter (which treats the crushed rock as a sphere) was used. Additionally, by knowing the actual area of the crushed rock, determined using the X-ray Computed Tomography method, it was decided to also calculate the *Nu* number for the crushed rock by inserting the actual area into Equation (12). The obtained results of the *Nu* number during the charging of the bed storage are shown in Figure 8.

The comparison of the characteristics of the *Nu* number for the charging process of the bed storage filled with spheres and crushed rock presented in Figure 8 shows that the nature of heat transfer is different for these geometries. Throughout the entire duration of the measurements, the *Nu* number for the spheres was always lower than for the crushed rock for all the analysed rates of airflow through the bed storage. It is worth noting that the *Nu* number for crushed rock has the highest values between the 50th and 100th minute of the research. The maximum value appears later with an increase in the airflow rate. For the granite, the maximum value occurs at the beginning of the process. As the air flow rate increases, the nature of the curve changes, and the time of the occurrence of the highest *Nu* number changes only for the highest flow. The introduction to the calculations of the actual crushed rock surface only partially brought the curve of the *Nu* number for the crushed rock closer to the curve for the sphere. However, it did not change its character. The *Nu* number for the crushed rock for which the actual surface was entered takes values lower than for the spheres in the first minutes of the measurements. The *Nu* value then increases, and follows the change in the *Nu* number for the crushed rock for which the surface was determined in the same way as for the sphere.

In order to formulate more general conclusions for different measurement series, it is worth using dimensionless parameters. One of the most frequently analysed relationships is $Nu = f(Re)$, which shows the effect of the movement of fluid on the heat transfer rate. This relationship is shown in Figure 9. The diagram shows the results of the tests for the sphere, crushed rock, and also for the crushed rock with its actual surface taken into account.

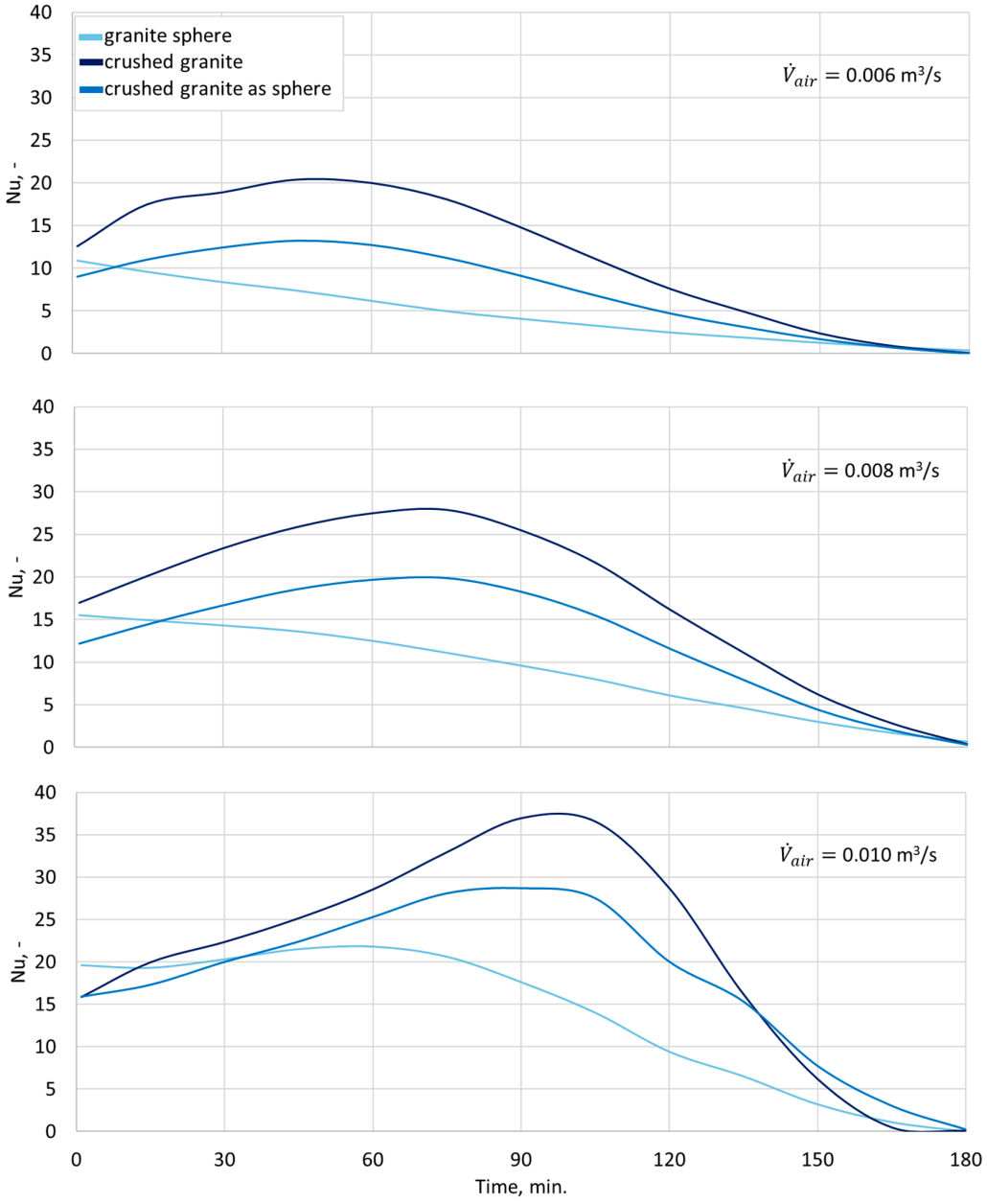

Figure 8. The Nusselt number during the charging process of the bed storage filled with granite.

The calculations assume that air is treated as a semi-perfect gas and that its physical properties are a function of temperature. Therefore, the obtained value of the *Re* number was variable for each of the flow rates during the measurements. Higher values of the *Re* number occurred at the beginning of the measurements, and these values decreased during the measurements. Large discrepancies in the *Nu* number, which are visible in Figure 8, can also be found in the graph of $Nu = f(Re)$. However, in the final phase of the research, the *Re* number for the sphere and crushed rock takes almost the same values for each of the settings. This is the result of similar values of the fluid temperature inside the bed storage. In the case of the sphere and crushed rock studies, the maximum value of the *Nu* number increases with an increase in the *Re* number. However, the highest values of the *Nu* number for the sphere are much lower than those for the crushed rock. Even the introduction of the actual crushed rock surface into the calculations did not lower the value of the *Nu* number to the level of the values obtained for the spheres. Moreover, the nature of the change in the *Nu* number is different for these geometries.

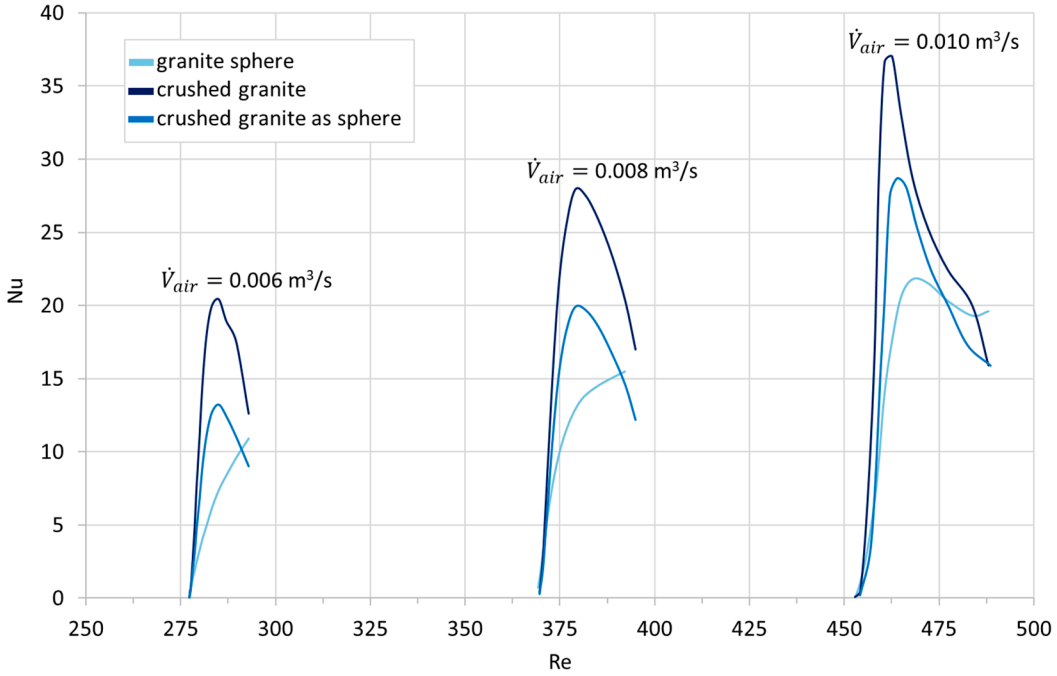

Figure 9. The dependence between the Nusselt number and the Reynolds number during the charging process of the bed storage filled with granite.

4. Discussion and Conclusions

As mentioned in the introduction, most of the work is focused on the discharge process and long-term charging of the heat storage. The conducted research showed that after the charging time of about 3 h, the outlet air temperature for the sphere is close to the temperature for the crushed rock. For the flow of 0.006 m^3/s, it differs by 1.9%; for the flow of 0.008 m^3/s, it differs by 0.9%, and for the flow of 0.010 m^3/s, it differs by 2.1%. All the obtained discrepancies are within the measurement error limit. However, as can be seen from Figure 5, the greatest difference in the value of outlet air temperature occurs during the first hour of charging. The temperature of the air at the outlet for the crushed rock as a storage material is lower than for the sphere. For the lowest flow it is lower by 40.4%, for the average flow it is lower by 22.0% and for the highest flow it is lower by 18.5%. These values exceed the maximum error resulting from the accuracy of the measuring devices. However, when the heat source cooperating with the bed storage supplies heat for short periods of time, or with breaks, it is important to know the process in the first hours of charging. Some of the information is obtained using model calculations. They take into account the amount of heat supplied to the bed storage and the losses from the surface of the tank. The process of heat penetration into the storage material is described by the heat transfer coefficient, which depends on the Nusselt number. Available equations describing the heat transfer process are used, and computational algorithms are created. However, the criterion equations available in literature for the *Nu* number of heat transfer into a bed storage, such as those summarized in Table 5, assume that parameters such as the equivalent diameter and the area of crushed rock are determined in the same way as for a sphere. This means that the model calculations performed with the use of these equations give the same results for the crushed rock as for the sphere.

The conducted research showed that there are clear differences in the heat transfer to the storage material with different geometries. This affects the temperature of the storage material. In the case of the performed tests, the temperature of the spheres was always lower than in the case of the crushed rock. After three hours of charging, it was lower by 25.2% for the flow of 0.006 m^3/s, 12.3% for the flow of 0.008 m^3/s, and 8.6% for the flow of 0.010 m^3/s. It is worth noting that the Nusselt number, which characterizes the process of heat transfer into the material, assumed almost the same values at the end of the measurements. However, the biggest differences were found in the second hour of

charging. The Nu number was greater for the crushed rock - for the lowest flow by 222.6%, for the average flow by 151.4%, and for the highest flow by 161.3%. The introduction of the correction in the form of taking into account the actual surface of the crushed rock only partially approximates the results obtained for the crushed rock. This proves that the larger actual surface of the crushed rock has an impact on the calculation result, and that its determination by treating the crushed rock as spheres causes erroneous results to be obtained. However, as the analysis shows, it is not the only factor that determines the intensity of the charging process of the heat storage. It is worth paying attention to the streamlined shape of the sphere, which is opposite to the shape of the crushed rock. This fact causes a less turbulent flow in the case of the sphere, which in turn reduces heat transfer. Moreover, equations 1 to 10 in Table 5 treat the heat transfer process very generally. Only in equation 11 was the correction for the filling factor of the heat storage introduced, and importantly, the correction resulted from the difference of the actual material surface in relation to the sphere. The conducted research leads to the conclusion that the mathematical description of heat transfer into the storage material could contain more parameters that determine the process, such as e.g., a material's roughness or sphericity. The created models, due to the increasing role of stored heat, would then better reflect this process from the very beginning.

Table 5. Selected Nusselt number formulas for packed beds.

No.	Dimensionless Equation		Notes	Ref.
1	$Nu_w = 2 + 1.8 \cdot Re^{0.5} \cdot Pr^{1/3}$	(16)	$100 \leq Re$ Pr for typical gases and liquids	[16]
2	$Nu_w = 2 + 1.1 \cdot Re^{0.6} \cdot Pr^{1/3}$	(17)	$15 \leq Re \leq 8500$	[40]
3	$Nu_w = 3.22(Re \cdot Pr)^{1/3} + 0.117 \cdot Re^{0.8} \cdot Pr^{0.4}$	(18)	$40 < Re$	[41]
4	$Nu_w = \frac{Re \cdot Pr^{1/3}}{\varepsilon}\left(0.0108 + \frac{0.929}{Re^{0.58} - 0.483}\right)$	(19)	$20 < Re$	[42]
5	$Nu_{eq} = \frac{Pr^{1/3}}{\varepsilon}\left(2.876 + 0.3023 \cdot Re_{eq}^{0.65}\right)$	(20)	$10 < Re_{eq}$	[43]
6	$Nu_w = 0.29 \cdot Re^{0.8} \cdot Pr^{1/2}$	(21)	$Re \leq 2400$	[44]
7	$Nu_w = 2 + 1.354 \cdot Re^{\frac{1}{2}} \cdot Pr^{\frac{1}{3}} + 0.0326 \cdot Re \cdot Pr^{1/2}$	(22)	$60 \leq Re$	[45]
8	$Nu_w = 2 + 0.6 \cdot Re^{0.5} \cdot Pr^{1/3}$	(23)	$1 \leq Re \leq 70{,}000$ $0.6 \leq Pr \leq 400$	[46]
9	$Nu_w = 0.8 \cdot Re^{0.7} \cdot Pr^{0.33}$	(24)	$500 \leq Re \leq 50{,}000$	[45]
10	$Nu_w = 2 + 0.03 \cdot Re^{0.54} \cdot Pr^{\frac{1}{33}} + 0.35 \cdot Re^{0.58} \cdot Pr^{0.356}$	(25)	-	[47]
11	$Nu_w = 0.437 \cdot Re^{0.75} \cdot \psi^{3.35} \cdot \varepsilon^{-1.62} \cdot [exp\{29.03(log\psi)^2\}]$	(26)	$\varepsilon^{*} = \frac{V_b - V_s}{V_b}$ $\psi^{**} = \frac{a_s}{a_c}$	[19]

* ε is the filling factor of the packed bed with air, V_b is the bed volume, V_s is the volume of the filler material, ** ψ is the area ratio, a_s is the area of the sphere, and a_c is the area of the selected material.

Finally, it is worth noting that the range of settings that are adapted to the cooperation between the bed storage and heat sources, such as solar air collectors, was tested. It is worth extending these tests in order to include higher flow rates of the working medium and higher temperatures. Moreover, it is worth checking the influence of the model describing heat losses on the uncertainty of the results, e.g., by using additional heat flux sensors.

Funding: This research was funded by The National Science Centre in Poland, grant number 2018/02/X/ST8/02938, and partly supported by the internal research funds of the Department of Thermodynamics and Renewable Energy Sources at Wroclaw University of Science and Technology, Poland, No. 8201003902 (MPK 9090750000).

Conflicts of Interest: The author declares no conflict of interest.

References

1. Gautam, A.; Saini, R.P. A review on technical, applications and economic aspect of packed bed solar thermal energy storage system. *J. Energy Storage* **2020**, *27*, 101046. [CrossRef]
2. Ergun, S.; Orning, A.A. Fluid Flow through Randomly Packed Columns and Fluidized Beds. *Ind. Eng. Chem.* **1949**. [CrossRef]

3. Esence, T.; Bruch, A.; Molina, S.; Stutz, B.; Fourmigué, J.F. A review on experience feedback and numerical modeling of packed-bed thermal energy storage systems. *Sol. Energy* **2017**, *153*, 628–654. [CrossRef]
4. Koçak, B.; Fernandez, A.I.; Paksoy, H. Review on sensible thermal energy storage for industrial solar applications and sustainability aspects. *Sol. Energy* **2020**, *209*, 135–169. [CrossRef]
5. Atalay, H. Assessment of energy and cost analysis of packed bed and phase change material thermal energy storage systems for the solar energy-assisted drying process. *Sol. Energy* **2020**, *198*, 124–138. [CrossRef]
6. Palacios, A.; Barreneche, C.; Navarro, M.E.; Ding, Y. Thermal energy storage technologies for concentrated solar power—A review from a materials perspective. *Renew. Energy* **2020**, *156*, 1244–1265. [CrossRef]
7. Kumar, A.; Kim, M.H. Solar air-heating system with packed-bed energy-storage systems. *Renew. Sustain. Energy Rev.* **2017**, *72*, 215–227. [CrossRef]
8. Mohana, Y.; Mohanapriya, R.; Anukiruthika, T.; Yoha, K.S.; Moses, J.A.; Anandharamakrishnan, C. Solar dryers for food applications: Concepts, designs, and recent advances. *Sol. Energy* **2020**, *208*, 321–344. [CrossRef]
9. Bazgaou, A.; Fatnassi, H.; Bouharroud, R.; Elame, F.; Ezzaeri, K.; Gourdo, L.; Wifaya, A.; Demrati, H.; Tiskatine, R.; Bekkaoui, A.; et al. Performance assessment of combining rock-bed thermal energy storage and water filled passive solar sleeves for heating Canarian greenhouse. *Sol. Energy* **2020**, *198*, 8–24. [CrossRef]
10. König-Haagen, A.; Höhlein, S.; Brüggemann, D. Detailed exergetic analysis of a packed bed thermal energy storage unit in combination with an Organic Rankine Cycle. *Appl. Therm. Eng.* **2020**, *165*, 114583. [CrossRef]
11. Singh, H.; Saini, R.P.; Saini, J.S. A review on packed bed solar energy storage systems. *Renew. Sustain. Energy Rev.* **2010**, *14*, 1059–1069. [CrossRef]
12. Berrhazi, S.; Ouammi, A.; Benchrifa, R. Thermo-physical effect of solid filler on the performance of a packed-bed thermal storage. *Therm. Sci. Eng. Prog.* **2020**, *20*, 100716. [CrossRef]
13. Gautam, A.; Saini, R.P. Experimental investigation of heat transfer and fluid flow behavior of packed bed solar thermal energy storage system having spheres as packing element with pores. *Sol. Energy* **2020**, *204*, 530–541. [CrossRef]
14. Nemś, M.; Nemś, A.; Pacyga, P. A granite bed storage for a small solar dryer. *Materials* **2018**, *11*, 1969. [CrossRef] [PubMed]
15. Nemś, M.; Nemś, A.; Gębarowska, K. The Influence of the Shape of Granite on the Heat Storage Process in a Rock Bed. *Energies* **2020**, *13*, 5662. [CrossRef]
16. Ranz, W.E.; Marshall, W.R. Evaporation from drops. Parts I & II. *Chem. Eng. Prog.* **1952**. [CrossRef]
17. Melissari, B.; Argyropoulos, S.A. Development of a heat transfer dimensionless correlation for spheres immersed in a wide range of Prandtl number fluids. *Int. J. Heat Mass Transf.* **2005**, *48*, 4333–4341. [CrossRef]
18. Kunii, D.; Levenspiel, O. *Fluidization Engineering*, 2nd ed.; Elsevier: Amsterdam, The Netherlands, 1991; ISBN 0-409-90233-0.
19. Singh, R.; Saini, R.P.; Saini, J.S. Nusselt number and friction factor correlations for packed bed solar energy storage system having large sized elements of different shapes. *Sol. Energy* **2006**, *80*, 760–771. [CrossRef]
20. Singh, H.; Saini, R.P.; Saini, J.S. Performance of a packed bed solar energy storage system having large sized elements with low void fraction. *Sol. Energy* **2013**, *87*, 22–34. [CrossRef]
21. Allen, K.G.; von Backström, T.W.; Kröger, D.G. Rock bed pressure drop and heat transfer: Simple design correlations. *Sol. Energy* **2015**, *115*, 525–536. [CrossRef]
22. Allen, K.G.; von Backström, T.W.; Kröger, D.G. Packed bed pressure drop dependence on particle shape, size distribution, packing arrangement and roughness. *Powder Technol.* **2013**, *246*, 590–600. [CrossRef]
23. Barton, N.G. Simulations of air-blown thermal storage in a rock bed. *Appl. Therm. Eng.* **2013**, *55*, 43–50. [CrossRef]
24. De la Beaujardiere, J.-F.P.; von Backström, T.W.; Reuter, H.C.R. Applicability of the local thermal equilibrium assumption in the performance modelling of CSP plant rock bed thermal energy storage systems. *J. Energy Storage* **2018**, *15*, 39–56. [CrossRef]
25. Soprani, S.; Marongiu, F.; Christensen, L.; Alm, O.; Petersen, K.D.; Ulrich, T.; Engelbrecht, K. Design and testing of a horizontal rock bed for high temperature thermal energy storage. *Appl. Energy* **2019**, *251*, 113345. [CrossRef]
26. Hailu, G.; Hayes, P.; Masteller, M. Long-term monitoring of sensible thermal storage in an extremely cold region. *Energies* **2019**, *12*, 1821. [CrossRef]

27. Allen, K.G.; Von Backström, T.W.; Kröger, D.G.; Kisters, A.F.M. Rock bed storage for solar thermal power plants: Rock characteristics, suitability, and availability. *Sol. Energy Mater. Sol. Cells* **2014**, *126*, 170–183. [CrossRef]
28. Marongiu, F.; Soprani, S.; Engelbrecht, K. Modeling of high temperature thermal energy storage in rock beds—Experimental comparison and parametric study. *Appl. Therm. Eng.* **2019**, *163*, 114355. [CrossRef]
29. Yang, B.; Bai, F.; Wang, Y.; Wang, Z. Study on standby process of an air-based solid packed bed for flexible high-temperature heat storage: Experimental results and modelling. *Appl. Energy* **2019**, *238*, 135–146. [CrossRef]
30. Jemmal, Y.; Zari, N.; Maaroufi, M. Experimental characterization of siliceous rocks to be used as filler materials for air-rock packed beds thermal energy storage systems in concentrated solar power plants. *Sol. Energy Mater. Sol. Cells* **2017**, *171*, 33–42. [CrossRef]
31. Heller, L.; Gauché, P. Modeling of the rock bed thermal energy storage system of a combined cycle solar thermal power plant in South Africa. *Sol. Energy* **2013**, *93*, 345–356. [CrossRef]
32. Ozturk, M.; Dincer, I.; Javani, N. Thermodynamic modeling of a solar energy based combined cycle with rock bed heat storage system. *Sol. Energy* **2020**, *200*, 51–60. [CrossRef]
33. Tuttle, J.F.; White, N.; Mohammadi, K.; Powell, K. A novel dynamic simulation methodology for high temperature packed-bed thermal energy storage with experimental validation. *Sustain. Energy Technol. Assess.* **2020**, *42*, 100888. [CrossRef]
34. Esence, T.; Bruch, A.; Fourmigué, J.F.; Stutz, B. A versatile one-dimensional numerical model for packed-bed heat storage systems. *Renew. Energy* **2019**, *133*, 190–204. [CrossRef]
35. Nemś, M.; Kasperski, J. Experimental investigation of concentrated solar air-heater with internal multiple-fin array. *Renew. Energy* **2016**, *97*. [CrossRef]
36. Bellos, E.; Tzivanidis, C. Alternative designs of parabolic trough solar collectors. *Prog. Energy Combust. Sci.* **2019**, *71*, 81–117. [CrossRef]
37. Kalinowski, E. *Termodynamika*; Wydawnictwo Politechniki Wrocławskiej: Wrocław, Poland, 1994; ISBN 83-7085-063-4. (In Polish)
38. Cengel, Y.A. *Heat Transfer: A Practical Approach*, 2nd ed.; McGraw-Hill: New York, NY, USA, 2002; ISBN 9780072458930.
39. Cengel, Y.A.; Boles, M.A. *Thermodynamics: An Engineering Approach*, 8th ed.; McGraw-Hill: New York, NY, USA, 2014; ISBN 9780073398174.
40. Wakao, N.; Funazkri, T. Effect of fluid dispersion coefficients on particle-to-fluid mass transfer coefficients in packed beds. Correlation of sherwood numbers. *Chem. Eng. Sci.* **1978**, *33*, 1375–1384. [CrossRef]
41. Beek, J. Design of Packed Catalytic Reactors. *Adv. Chem. Eng.* **1962**. [CrossRef]
42. Gupta, A.S.; Thodos, G. Mass and heat transfer in the flow of fluids through fixed and fluidized beds of spherical particles. *AIChE J.* **1962**, *8*, 608–610. [CrossRef]
43. Gupta, S.N.; Chaube, R.B.; Upadhyay, S.N. Fluid-particle heat transfer in fixed and fluidized beds. *Chem. Eng. Sci.* **1974**, *29*, 839–843. [CrossRef]
44. Nield, D.A.; Bejan, A. *Convection in Porous Media*, 3rd ed.; Springer: New York, NY, USA, 2006; ISBN 9780387290966.
45. Beasley, D.E.; Clark, J.A. Transient response of a packed bed for thermal energy storage. *Int. J. Heat Mass Transf.* **1984**. [CrossRef]
46. Kostowski, E. *Zbiór Zadań z Przepływu Ciepła*; Wydawnictwo Politechniki Śląskiej: Gliwice, Poland, 2006; ISBN 83-88000-18-7. (In Polish)
47. Domański, R. *Magazynowanie Energii Cieplnej*; Państwowe Wydawnictwo Naukowe: Warsaw, Poland, 1990; ISBN 8301093978. (In Polish)